A Vision-based Controller for Path Tracking of Autonomous Underwater Vehicles

Carlos Berger[1,2],Mario A. Jordán [1,2,⋆], Jorge L. Bustamante[1,2] and Emanuel Trabes [1]

[1] Argentinean Institute of Oceanography (IADO-CONICET).
Florida 8000, Complejo CCT, Edificio E1, B8000FWB,
Bahía Blanca, ARGENTINA.

[2] Dto. Ingeniería Eléctrica y de Computadoras- Univ. Nac. del Sur (DIEC-UNS).
No Institute Given

Abstract. This paper aims a design of a vision-based controller for autonomous underwater vehicles (AUVs). The control system performs the path following of a line on the seafloor and tunes automatically the cruise kinematics for the advance.The navigation process rests upon a sensor which estimates the relative vehicle position from the perspective of the camera directly without the need of employing camera models for estimating physical variables. For the state estimation, image processing in real time is employed. The control strategy is developed in the state space of pure vision coordinates. The strategy points to reach rapidly favorable configurations of the AUV and afterwards to pursue a perfect alignment with the line. Experiments of the real subaquatic world are presented.

Key words: Autonomous underwater vehicle, Control and guidance systems, Path following, Vision sensor, Vision-based control.

1 Introduction

The interest for subaquatic vehicle applications is continuously increasing, driven above all by the high technological instrumentation available for underwater surveys and the highly advanced processing capabilities. Applications embrace not only the classical ones of the off-shore oil industry but also rescues, wide oceanographic and scientific missions (Narimani *et al.*, 2009).

One of the most relevant technical application concerns the pipeline tracking on the sea bottom with the goal of inspection and post-lay pipe surveys (Wadoo and Kachroo, 2010; Inzartev, 2009; Wang *et al.*, 2007; Foresti, 2001). This framework gives input to the main motivation of this paper in the framework of control systems with camera sensors.

Vision-based guidance systems with blurred imaging come into consideration principally in scenarios when the altitude to bottom is relatively small. Moreover, in such complex scenarios an intelligent sensor to identify the pipe on the sea floor with its particularities and a guidance system to follow it automatically

⋆ Corresponding Author: Mario A. Jordán: E-mail: mjordan@criba.edu.ar. Address: CCT-CONICET. Florida 8000, B8000FWB, Bahía Blanca, ARGENTINA

may be a useful complement of other navigation sensors (Jordán, 2010; Sattar *et al.*, 2008; Huster *et al.*, 2002).

In this paper, the design of a controller for path following with desired kinematics based on pure vision characteristics provided by a camera pointing to a line is described. It is stressed the absence of any model of the AUV dynamics in the controller design. Closing the paper, real experiments on an underwater scenario are illustrated.

2 Preliminary

Let us consider an AUV navigating at constant altitude h over a patterned line laid on a planar floor. Imagine a line stretch captured by the in-board camera like in the Fig. 1. The well known pin-hole camera model is considered (Hartley, 2004). Here, a line stretch is ideally described by its tangent line on a point, with parameters x_L (in pixel) and α (radian). Actually, the tangent line represents an approximation of a secant line which fits at best the orientation of the physical line in the frame. Moreover, the camera is placed at a distance d from the vehicle mass center and its orientation angle with respect to the vertical line is β. When the AUV is misaligned with the line, this can be characterized by a lateral shift Y_t of its mass center and an orientation angle ψ with respect to the tangent line, both defined in a line-fixed coordinate system (X_t, Y_t, Z_t) with X_t oriented along the line. These vision and the physical parameters are related by (see Berger, 2014a)

$$\begin{cases} Y_t = s_1 \sin\psi + s_2 x_L \cos\psi \\ tg\psi = s_3 tg\alpha + s_4 x_L \end{cases}, \tag{1}$$

with $s_1{=}d + h\tan\beta$, $s_2{=}\frac{-h}{f\cos\beta}$, $s_3{=}-\cos\beta$, $s_4{=}\frac{\sin\beta}{f}$,and f being the focal distance.

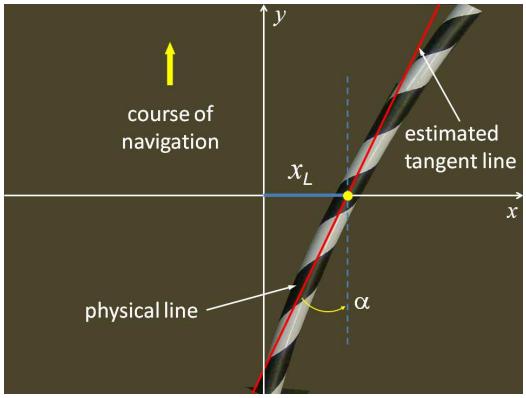

Fig. 1 - Camera frame with the physical patterned line and its approximated tangent line

Clearly, the equilibrium points $x_L = \alpha = 0$ and $Y_t = \psi = 0$ are arrived at the same time in different state spaces. So, the future control objective will be to force trajectories to the equilibrium $x_L = \alpha = 0$ in the vision state space only and to automatically establish kinematics references.

Let us consider a planar motion at constant altitude. Assume the vehicle has been constructed to rotate at about the mass center. Let Ω_{Z_M} be the angular

rate about the vertical axis Z and $\dot{X}_M$ the advance rate. It is shown in Berger (2014a) that the camera kinematics obeys to

$$\begin{bmatrix} \dot{x} \\ \dot{y} \end{bmatrix} = \begin{bmatrix} -Kd + f\left(1 + \frac{x^2}{f^2}\right)\sin(\beta) + y\cos(\beta) & x\sin(\beta)\frac{K}{f} \\ -xK\frac{h}{f} & -K\cos(\beta) + K\frac{y}{f}\sin(\beta) \end{bmatrix} \begin{bmatrix} \Omega_{Z_M} \\ \dot{X}_M \end{bmatrix} \tag{2}$$

where

$$K = \frac{f}{Z} = \frac{f\cos(\beta) - y\sin(\beta)}{h}.$$

3 Vision-based sensor

The core of the guidance system and control feedback is the sensor. It carries out the image processing in order to estimate the camera position and its kinematics with respect to the seafloor. It also enable the construction of kinematics references in order to achieve an adequate vehicle advance in the path tracking. Finally, a monitoring of the quality of the estimations constitutes another output of the sensor. Taken the hardware capacities into account (*e.g.*, frame-grabber and mini PC-platform), the frames are processed at a rate of $c \cdot fps$, where fps is the frame per second property of the camera and $0 < c < 1$ defines a subsampling rate. The different modules concerning the sensor functioning are depicted in the following figures. These are executed successively each $1/(c \cdot fps)$ seconds.

The first module is summarized in Fig. 2. It contains the estimation of the relative vehicle position to the line in the vision space through the parameters x_L and α. The first step is to improve the quality of the raw frame in order to enhance the contrast between patterns and environment and to get an image segmentation of these regions. Then, one extracts image features that ends with the determination of pattern centroids of the line. The reasonable ambiguity of the estimation is delimited by defining a certainty zone around it.

In Fig. 3 the second module is presented. It performs the estimation of the camera motion first and the vehicle motion in the following. The key idea is to calculate a velocity field over the identified centroids of the previously segmented set of patterns in two successive frames and then to employ this velocities to solve (2) in order to estimate $\dot{X}_M$ and Ω_{Z_M}, or equivalently in the vehicle-fixed coordinate system: u and r, respectively.

The first step in this module consists in attaining the maximal number of centroids as possible from both frames. So, eventual holes that are originated from lost patterns may be recognized to enhance the sets. Here, their coherence with eventual logical metrics-calculated positions enables to interchange holes by simulated centroids.

The rate field of the centroids is worked out by overlapping the directrix lines of the centroid sets. The way this is done consists in rotating one directrix line to the other around the crosspoint in order to get them parallel. In this form, homologous centroids can be associated by a distance representation with respect to the crosspoint (the *ad-hoc* origin) in order to construct pairs. Finally the rate field results from the ratio between the distances of each pair centroids $(\dot{x}, \dot{y})$ and the period $1/(c \cdot fps)$. In order to reduce the influence of numeric errors in the estimation of the vehicle rate variables $\dot{X}_M$ and Ω_{Z_M}, (2)

is solved for the estimated pairs in the sense of a least squares metrics. Additionally the centroid positions suffer from quantification errors and false perspective appreciation which are common in 2D-image approaches. So the evolution of the estimates may be irregular and a *ad-hoc* filtering is needed.

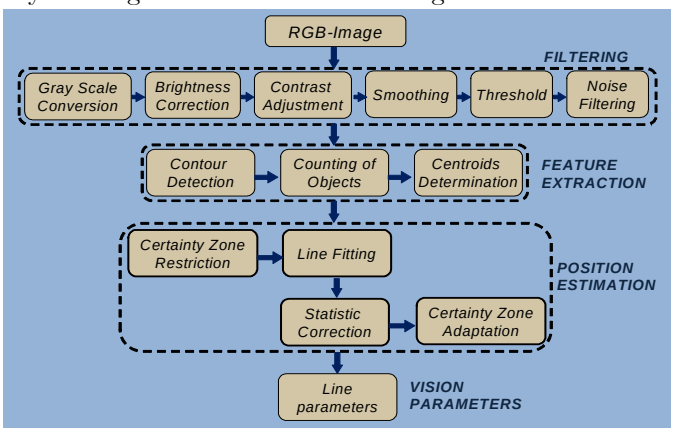

Fig. 2 - Sensor module I: position estimation

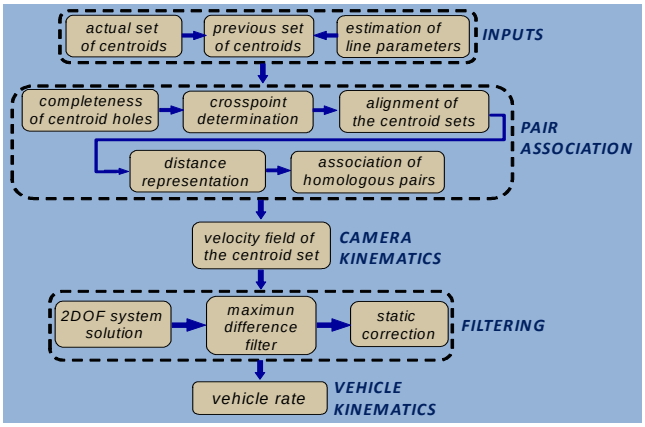

Fig. 3 - Sensor module II: kinematics estimation

To this end, a so-called maximum-difference filter is used to reduce high fluctuations due to elevated noise level (change of contrast, caustic waves, etc.). Finally, average in time with a forgetting factor is necessary to smooth the rate estimations that are affected from erratic centroid shifts. This step ends the estimation of the vehicle motion.

In Fig. 4, the third sensor module is described. Herein, the real-time monitoring of the sensor performance is produced in order to alert the controller when the sensor is momentarily unreliable. In this sense, the controller will have to take extra actions for the continuity of the navigation. In customary operations, pattern estimations may fail, for instance due to sporadic bad image quality (in cloudy waters or in the presence of caustic waves) or simply when patterns ran over the frame (due to strong force perturbations).

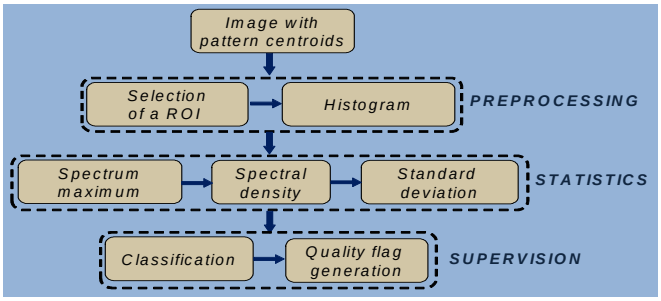

Fig. 4 - Sensor module III: sensor performance supervision

The strategy in the real-time supervision task consists in analyzing the statistical properties of a selected ROI in the certainty zone. Then its histogram parameters (spectral density and maxima, standard deviation) are compared with those of the seafloor which has been collected in a calibration phase. It is expected that the line histogram looks approximately like a bimodal function, while the floor (which is generally dark) has a rather one-peak histogram.

4 Controller Design

The line tracking is enabled by the guidance and control system. They are illustrated in Fig. 5. The sensor acts as the navigation system. No other information than the estimated position (x_L, α) and vehicle rate (u, r) is employed to generate velocity references (u_{ref}, r_{ref}) and control actions (here termed the force τ_u and the moment τ_r to cause push/braking and turn, respectively).

Whereas an ideal controller has to maintain all the time the line vertically on the middle of the screen (*i.e.* at the desired position x_L=α=0), a good controller however will attempt to achieve this goal asymptotically after a sporadic perturbation or more practically, by forcing the track errors to be small during a curve path. It is also stipulated that the vehicle achieves a nominal cruise rate u_{nom} when it is well aligned with the line. The actual reference velocity (generally lower than u_{nom}) will depend on its misalignment with respect of the line.

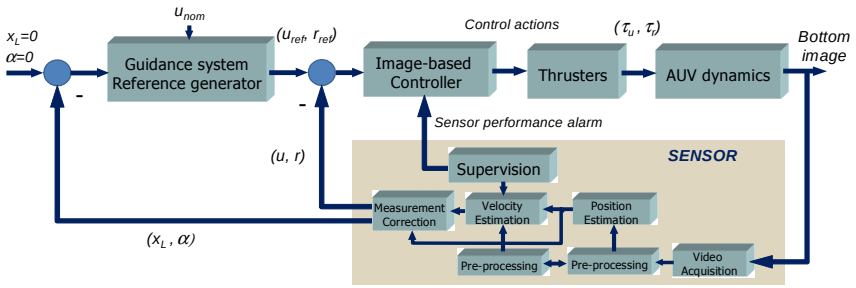

Fig. 5 - Vision-based control system

The control strategy is constructed on the vision state space (see Fig. 6), in where position trajectories evolve from an initial condition to the equilibrium point x_L=α=0 of the perfect alignment.

Basically the space is delimited by the visibility of the line segment in the frame. So, when the segment stays on the contour of the frame (i.e., one of the

four sides or one of the four corners), then the line is described by a point on one of the four curves α_{LIM_i}. On the other side, it is practical for the control to restrict de angle α in an interval, it is $-\pi/2<\alpha_{MIN} \leq \alpha \leq \alpha_{MAX}<\pi/2$ to avoid ambiguity in the orientation sense with respect to the current course of navigation.

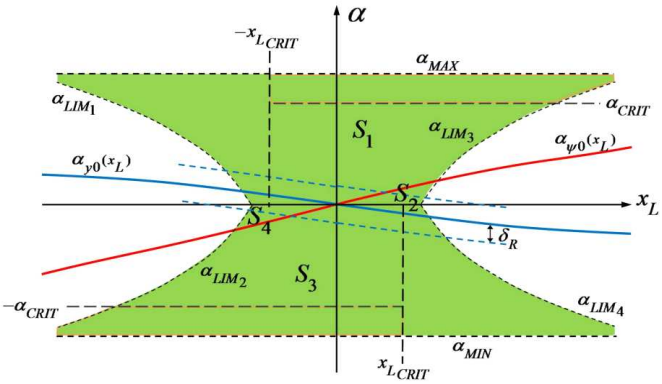

Fig. 6 - Vision state space for the control strategy

When mapping the four quadrants of the physical space (Y_t, ψ) into the vision space by means of (1), it originates four regions identified as S_1, S_2, S_3 and S_4 delimited by two contour curves, namely $\alpha_{y0}(x_L)$ (*i.e.*, the map for Y_t=0) and $\alpha_{\psi 0}(x_L)$ (*i.e.*, the map for ψ=0), which clearly represent the maps of the orthogonal axes of the physical plane (Y_t, ψ). The AUV positions depicted in Fig. 7 corresponds to these particular cases pointed out before.

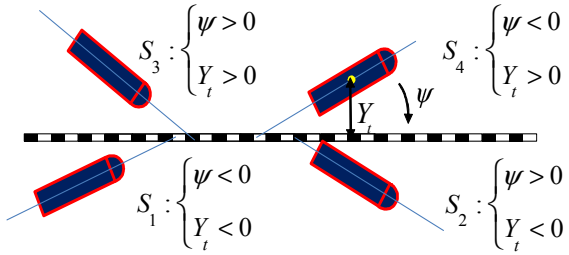

Fig. 7 - AUV positions in the four quadrants of the physical space

Clearly, regions S_2 and S_4 are smaller in size than S_1 and S_3 because the sight horizon is shorter when the AUV camera is located on the AUV nozzle. Another restrictions on the vision space arrives from the control strategy. The cause for further subdivisions on the plane rests on the fact that the controller design does not employ any model of the AUV dynamics. So, when the AUV stays both close to the vision limits or close to the equilibrium point, it is reasonable to diminish the energy amount of the control efforts in order to cause a lower motion quantity. In this sense, it appears appropriate first to define narrower limits on x_L and α, namely $\pm x_{L_{CRIT}}$ and $\pm \alpha_{CRIT}$. Additionally, in a neighborhood of the equilibrium point, it seems cautious to diminish the controller gain when the vehicle stays approximately aligned with the line. So, in this case a kind of corridor is defined for small lateral displacements with wide equal to $2\delta_R$.

5 Guidance and control system

5.1 Guidance

The guidance law is worked out on the basis of the following idea. The more directly the vehicle aims to the line the more cautious is the guidance system to push it going through the line. So, when the vehicle brings closer to the line, the energy amount to decelerate it is relative small. Conversely, by closer alignment, the guidance system speed up the course. With this argument, we propose the reference law for the advance velocity

$$u_{ref} = \frac{u_{nom}}{(1 + K_c\psi^2)}, \tag{3}$$

with K_c a positive real-valued constant (*cf.,* Fig. 5). Another particularity of the control strategy is defined when the vehicle is far away to the line. The first attempt of the controller is to direct the vehicle with a constant angle ψ in order to diminish the lateral error x_L as quick as possible. Only when the vehicle stays close the line, the controller forces the vehicle a turn appropriately. The reference rate r_{ref} is constructed as following.

First, we employ the well-known relation between lateral rates with respect to a line-fixed and a vehicle-fixed systems, namely $\dot{Y}_t = u \sin\psi$. Now we can establish a law for the desired turn as

$$\psi_d = \arcsin\left(\frac{\dot{Y}_{t_d} - k_y(Y_{t_d} - Y_t)}{u_{ref}}\right), \tag{4}$$

with $Y_{t_d} = \dot{Y}_{t_d} = 0$ and $k_y < 0$ which penalizes side errors. So, the following reference for guidance is proposed

$$r_{ref} = \dot{r}_d - k_\psi(\psi_d - \psi), \tag{5}$$

with $k_\psi < 0$ penalizing the orientation errors. Taking into account that

$$\dot{\psi} = r_{ref} = \dot{r}_d - k_\psi(\psi_d - \psi),$$
$$\dot{Y}_t = u_{ref}\sin\psi_d = u_{ref}\left(\frac{\dot{Y}_{t_d} - k_y(Y_{t_d} - Y_t)}{u_{ref}}\right)$$

and defining $\tilde{\psi} = \psi_d - \psi$ and $\tilde{Y}_t = Y_{t_d} - Y_t$, one arrives to the error dynamics as

$$-\dot{\tilde{\psi}} + k_\psi\tilde{\psi} = 0, \qquad -\dot{\tilde{Y}}_t + k_y\tilde{Y}_t = 0.$$

Clearly, the equilibrium point $\tilde{\psi} = \tilde{Y}_t = 0$ is exponentially stable.

However, the practicability of (3) and (5) is reduced since Y_t and ψ are unknown. Certainly, their estimation by means of (1) is viable but not recommended when the operation and camera parameters (f, β, h) are changeable or uncertain.

An alternative to design the guidance system is to employ directly a metrics in the vision state space which does not suffer from such uncertainties. To this goal, consider the space in Fig. 8 where any vehicle position point $\mathbf{h}$ is at distances $\bar{d}_R$ and $\bar{d}_T$ to the isolines $\alpha_{y0}(x_L)$ and $\alpha_{\psi 0}(x_L)$, respectively. Clearly, $\bar{d}_R$ and $\bar{d}_T$ are positions variables like the equivalent Y_t and ψ. Much easier to compute

than $\bar{d}_R$ and $\bar{d}_T$, are their projection distances onto the axis α, namely d_R and d_T. Consequently, the equilibrium point $\tilde{\psi}$=$\tilde{Y}_t$=0 occurs uniquely by d_R=d_T=0.

So, the guidance system is redesigned as following. The kinematics references are replaced by

$$\begin{aligned} u_{ref} &= \frac{u_{nom}}{(1+K_c d_T^2)}, \\ d_{T_d} &= \arcsin\left(\frac{\dot{d}_{R_d} - k_y(d_{R_d} - d_R)}{u_{ref}}\right), \\ r_{ref} &= \dot{d}_{T_d} - k_\psi(d_{T_d} - d_T), \end{aligned} \tag{6}$$

with $d_{R_d} = \dot{d}_{R_d} = \dot{d}_{T_d} = 0$.

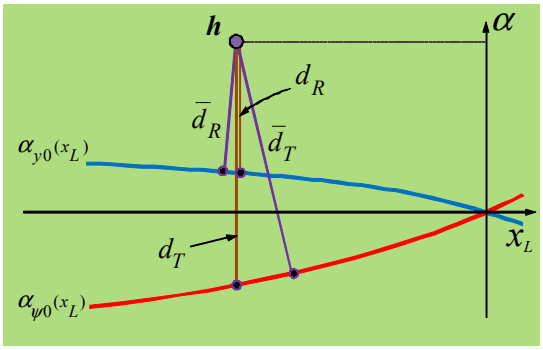

Fig. 8 - Vision-based metrics for position

5.2 Control strategy

The challenge now is to restrict the guidance law in such a manner that it be effective not only across the length and breadth of the vision space, but also in a neighborhood of the equilibrium point and in the periphery close to the vision contours. So we take up again the subdivisions of the space in Fig. 6 according to the limits $\alpha_{MIN}, \alpha_{MAX}$, α_{CRIT}, $x_{L_{CRIT}}$ and finally the corridor $2\delta_R$ wide.

In consequence, the control law is region-dependent with different mathematical expressions each one. This means that the vehicle can be propelled or stopped when trespassing the contours between two regions, diminishing or accentuating the rate of navigation. In short, the bandwidth of the controller is variable. For instance, subtle refinements of the track are necessary in the neighborhood of the equilibrium point, while strong thrusts are required in peripheral vision zones when the line is about to disappear from the image.

Accordingly we define the control strategy involving three laws for implementing the guidance.

Guidance law 1 - Risk of line loosing

On the condition $|\alpha| > |\alpha_{CRIT}|$, the strategy consists in generating a rotation in order to approach the isoline $\alpha_{\psi 0}(x_L)$. Consequently, we choose the desired value $d_{T_d} = 0$ and so (6) get into

$$\begin{aligned} u_{ref} &= \frac{u_{nom}}{(1+K_c d_T^2)}, \\ r_{ref} &= \dot{d}_{T_d} + k_\psi d_T. \end{aligned} \tag{7}$$

Guidance law 2 - Vehicle is almost aligned

If the trajectory fulfills for any point $\mathbf{h} \in \{S_1, S_3\}$ with $|x_L| > |x_{L_{CRIT}}|$ and $|d_R| > \delta_R$, the control strategy has to compel a movement that allows the vehicle to approach $\alpha_{y0}(x_L)$ and, at the same time, to be repulsed from the nearest limit α_{LIM}.

To attain both goals, d_D and d_I are defined as the distances of $\mathbf{h}$ to the line $x_L = x_{L_{CRIT}}$ if $x_L > 0$ or to $x_L = -x_{L_{CRIT}}$ if $x_L < 0$ and to the closest curve α_{LIM} (*i.e.,* α_{LIM1} in S_1 and α_{LIM4} in S_3).

Thus

$$d_D = \left| |x_L| - x_{L_{CRIT}} \right|,$$
$$d_I = \begin{cases} \left| |x_L| + \frac{H}{2}\tan\alpha - \frac{W}{2} \right| & \text{if } \mathbf{h} \in S_3 \\ \left| |x_L| - \frac{H}{2}\tan - \frac{W}{2} \right| & \text{if } \mathbf{h} \in S_1 \end{cases},$$

with W and H the number of pixels sideways and lengthways, respectively.

According to this metrics, the new guidance law is designed as

$$\hat{d_{T_d}} = k_r \left(1 + \frac{d_I - d_D}{d_I + d_D}\right) d_T, \tag{8}$$
$$d_{T_d} = \max(\min(\hat{d_{T_d}}, \alpha_{CRIT}), -\alpha_{CRIT}),$$
$$u_{ref} = \frac{u_{nom}}{(1 + K_c d_T^2)},$$
$$r_{ref} = \dot{d}_{T_d} - k_\psi (d_{T_d} - d_T),$$

with $0 < k_r < 1$. The heuristics behind (8) is the following. On one side, the quotient $(d_I - d_D)/(d_I + d_D)$ results in a real value in $[-1, 1]$. The minimum quotient value corresponds to the case $d_I = 0$ for $\mathbf{h}$ on one border α_{LIM}. So one gets $\hat{d}_{T_d} = k_r\,(1-1)\,d_T = 0$ and the guidance produces a rotation with the power enough to move $\mathbf{h}$ to the $\alpha_{\psi 0}(x_L)$. On the contrary, by $d_D = 0$ then it results the maximum quotient value, originating $\hat{d}_{T_d} = k_r 2 d_T$. In this way, the variation of the reference r_{ref} is gradual, namely it grows up in order to stop the rate until the sense of the rotation be changed. Particularly, with $k_r < 0.5$ one gets $k_r \left(1 + \frac{d_I - d_D}{d_I + d_D}\right) < 1$ and $\left|\hat{d}_{T_d}\right| < |d_T|$, causing a continuous repulsion of from the border α_{LIM} inside the interior region with $|x_{L_k}| < |x_{L_{CRIT}}|$.

Guidance law 3 - Vehicle is misaligned

Whenever $\mathbf{h}$ corresponds to other region that those circumvented in laws 1 and 2, the expression (6) applies with a saturation on d_{T_d} in order to avoid that the trajectories move into zones defined by $|\alpha| > \alpha_{CRIT}$. So

$$u_{ref} = \frac{u_{nom}}{(1 + K_c d_T^2)}, \tag{9}$$
$$\hat{d_{T_d}} = \arcsin\left(\frac{\dot{d}_{R_d} - k_y(d_{R_d} - d_R)}{u_{ref}}\right),$$
$$d_{T_d} = \max(\min(\hat{d_{T_d}}, \alpha_{CRIT}), -\alpha_{CRIT}),$$
$$r_{ref} = \dot{d}_{T_d} + k_\psi d_T.$$

Generally, all the laws attains the repulsion of the vehicle from the critical zones to inside and finally to the perfect alignment. However this occurs when the gains K_c, k_y, k_ψ and k_r have the signs as indicated. The tuning of these controller parameters pertains to a commissioning phase. The smaller the tracking errors $\tilde{\psi} = \psi_d - \psi$ and $\tilde{Y}_t = Y_d - Y_t$ the the more exact are the approximations d_T and d_R to ψ and Y_t, respectively.

5.3 Control law

The following of kinematics references provided by the guidance system are achieved by the vision-based controller which is connected in cascade in the direct path of the control system as depicted in Fig. 5.

The controller determines the thrust laws for a push and a rotation torque denominated τ_u and τ_r, respectively. The equations are defined on the basis of the kinematics errors $\tilde{u}$ and $\tilde{r}$ calculated upon the the sensor rate estimations $\hat{u}$ and $\hat{r}$. It is valid

$$\tau_u = K_{av}\tilde{u}, \qquad \tau_r = K_{rot}\tilde{r},$$

with $\tilde{u} = u_{ref} - \hat{u}, \tilde{r} = r_{ref} - \hat{r}$ and the controller gains $K_{av} > 0$ and $K_{rot} > 0$.

6 Experimental test

With the purpose of evaluating the performance of the vision-based control approach in scenes as close as possible to the real world, a series of experiments were carried out in a water tank with an experimental AUV (see Berger, 2014a; Berger, 2014b). Here, we present a case study employing a line with luminous patterns distributed uniformly along its length. The water scenario is characterized by a high turbidity and a poor natural illumination. As drawback in this conditions, the degree of blurring of the luminous points is very high. The submarine with the camera on board is directed approximately to the vision field over the line. As illustrated in Fig. 9, selected frames of the navigation are organized vertically from bottom (test start) to top (test end). To the left, the path of the submarine is indicated with reconstructed positions and orientations through the video. The triangle symbol in red illustrates samples of the AUV position. The line tracking is started from a favorable position (see first frame on the figure bottom). The supervision module indicates during the whole process that the track is successful by showing the specific symbol (circle in green) at the fram[illegible]

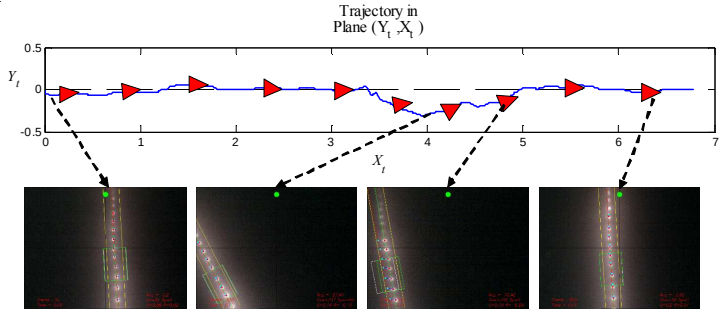

Fig. 9 - Case study of path tracking with side disturabances. Performance evaluation

In the middle of the navigation stretch, a strong force perturbation was externally exerted from one side on the submarine, moving it off the track. One sees on the vision field that the line begin to move rapidly to a corner (second frame from bottom) but the controller is able to recover the course immediately (third frame from bottom). In the final path, the controller is succeeding in improving the track precision increasingly (see the fourth frame from bottom).

The good performance of the control system can be also judged analyzing the time evolutions of the state variablesY_t, ψ, u, r, the approximations d_R and d_T and finally the thrusts τ_u and τ_r. All these are depicted in Fig. 10.

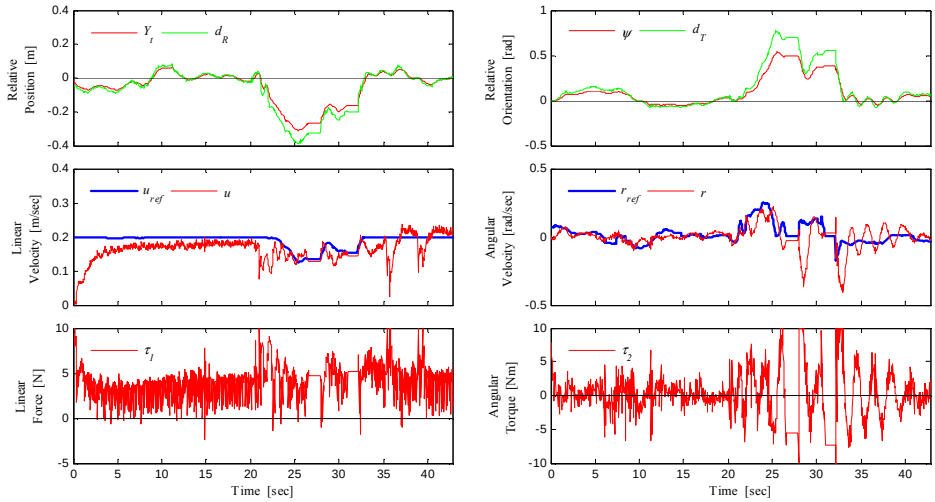

Fig. 10 - Time evolution of the state variables, references and thrusts

The null kinematics initial conditions cause the acceleration of the vehicle during $5s$ until the cruise velocity is approximately reached. At the start, the push and the torque evolve slightly jerky though their mean values are more significant to counteract the vehicle inertia. The reason is the form how the law does calculate the control actions by amplifying the path errors directly without filtering. On the other side, one sees the evolution of the vehicle by the force perturbation and the rapid control of the course with the cruise velocities. Finally, one can compare the evolution of the vision-based metrics through d_R and d_T, with the physical variables Y_t and ψ. Clearly, the small they are the most precise is the coincidence.

In Fig.11, the trajectories for position of the AUV in different metrics are depicted. One appreciates the great effect of the perturbation on the dynamics through the large separation of the trajectories with respect to the initial condition point. One notices how disimil are the trajectories in both spaces despite the fact that their convergences occur at the same point.

7 Conclusions

In this work a vision-based guidance and control system was presented for an AUV whose navigation system is constituted by a camera only. The design of

the sensor modules and controller were described. Also a case study, which was selected from of a series of experimental tests, was analyzed. In particular, the controller and the guidance system are based on a pure vision-based metrics, which, in theory, may present the advantage of not being influenced by parameter uncertainties like camera focus and altitude among others. This last hypothesis stays under verification in our future work. The all-round performance evaluated through experiments, has been ranged as good, robust and reliable in scenarios with cloudy waters and blurred images.

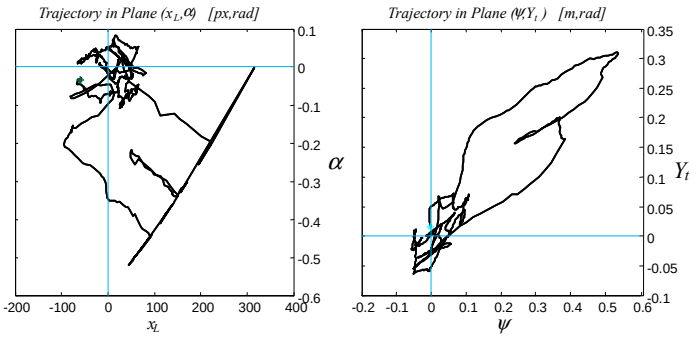

Fig. 11 - Time evolution of the state variables, references and thrusts

References

1. Berger, C. E. (2014a). PhD Thesis: *Navegación de Vehículos Autónomos Subacuáticos basados en Control por Visión*. Universidad Nacional del Sur, Argentina.
2. Berger, C. E. (2014b). Experimental video sequences: https://www.dropbox.com/sh/84woaxb5bklkboo/qeW3SoEjwf
3. Foresti, G.L. (2001). Visual inspection of sea bottom structures by an autonomous underwater vehicle. *In IEEE Trans. on Systems, Man, and Cybernetics, Part B: Cybernetics*, Vol. 31 (5), pp. 691-705.
4. Hartley, R. I. and Zisserman, A. (2004). *Multiple View Geometry in Computer Vision*, Cambridge University Press, ISBN: 0521540518.
5. Inzartev A.V.(Ed.) (2009). *Underwater vehicles*, InTech, Vienna, Austria.
6. Jordán, M.A., Berger, C.E., Bustamante, J.L. and Hansen, S. (2010). Path Tracking in Underwater Vehicle Navigation - On-Line Evaluation of Guidance Path Errors via Vision Sensor. *49th IEEE Conf. on Decision and Control*. Atlanta, USA.
7. Narimani, M., Nazem, S. and Loueipour, M. (2009). Robotics vision-based system for an underwater pipeline and cable tracker. *OCEANS'09*, Bremen, Germany, 1-6.
8. Sattar, J., Dudek, G., Chiu, O., Rekleitis, I., Giguere, P., Mills, A., Plamondon, N., Prahacs, C., Girdhar, Y., Nahon, M. and Lobos, J.-P. (2008). Enabling autonomous capabilities in underwater robotics. *In IEEE/RSJ Int. Conf. on Intelligent Robots and Systems (IROS 2008)*, Nice, France, pp. 3628-3634.
9. Wadoo, S. and Kachroo, P. (2010): *Autonomous Underwater Vehicles - Modeling, Control Design and Simulation*, CRC Press.
10. Wang, Y. and Hussein, I.I. (2007). Cooperative Vision-Based Multi-Vehicle Dynamic Coverage Control for Underwater Applications. *In IEEE Int. Conf. on Control Applications (CCA 2007)*, Singapore, pp. 82-87.